The Cryosphere

Discussions

The role of snow and ice thickness on river ice process in Songhua River basin, Northeast China

Qian Yang[1,2], Kaishan Song[1], Xiaohua Hao[3], Zhidan Wen[2], Yue Tan[1,] and Weibang Li[1]

[1]Jilin Jianzhu University, Xincheng Road 5088, Changchun 130118 China; E-Mail: jluyangqian10 @hotmail.com

[2] Northeast Institute of Geography and Agroecology, Chinese Academy of Sciences, Shengbei Street 4888, Changchun 130102 China; E-Mail: songks@neigae.ac.cn;

[3] Northwest Institute of Eco-Environment and Resources, Chinese Academy of Sciences, Donggang West Road 322, Lanzhou 730000, China; E-Mail: haoxh@lzb.ac.cn;

Correspondence to: Song K. S. (songks@neigae.ac.cn)

Abstract: Songhua River basin is a sensitive area to global warming in Northeast China that could be indicated by changes in lake and river ice development. The regional role and trends of ice characteristics of this area have been scarcely investigated, which are critical for aquatic ecosystem, climate variability, and human activities. Based on the ice record of hydrological stations, we examined the spatial variations of the ice phenology and ice thickness in Songhua River basin in Northeast China from 2010 to 2015 and explored the role of ice thickness, snow during ice-on and ice-off process. All five river ice phenology including freeze-up start, freeze-up end, break-up start, break-up end and complete frozen duration showed latitudinal distribution and a changing direction from southeast to northwest, and five typically geographic zones were identified based on rotated empirical orthogonal function. Maximum ice thickness had a higher correlation with five parameters than that of average snow depth and air temperature on bank. A linear regression function was established between ice thickness and snow depth on ice and indicated ice thickness was closely associated with snow depth on ice. The air temperature had higher correlation with ice phenology and influenced the lake ice phenology significantly, and snow cover did not show significant correlation with the ice phenology. However, snow cover correlated with ice thickness significantly and positively during the periods when the freshwater is completely frozen.

Keywords. River ice, ice phenology, ice thickness, snow on ice, air temperature, rotated empirical orthogonal function

1 Introduction

The freeze and thaw process of surface ice of temperate lakes and rivers plays crucial roles in the interaction among climate system (Stephanie and Stefan Heinz, 2006), freshwater ecosystem (Kwok and Fahnestock, 1996) and biological environment. The existence of freshwater ice closely associate with social and economic activities ranging from human-made structures, water transportation to winter recreation (Lindenschmidt et al., 2017; Williams and Stefan, 2006). The ice cover on rivers and lakes has exerted large forces due to thermal expansion and could cause extensive loss of the human-made structures, such as bridges, docks, shorelines, and so on (Shuter et al., 2012). Furthermore, ice cover on waterbodies provide a natural barrier between the atmosphere and the water and blocks the solar radiation necessary for photosynthesis and enough dissolved oxygen for fish, which have a negative effect on freshwater ecosystem, in extreme cases, leading to winter kills of fishes (Hampton et al., 2017; Xing et al., 2009). Generally, the frozen duration of freshwater ice has

40 a shorten trend with later freeze-up and earlier break-up throughout the northern hemisphere, *i.e.,* with freeze-up date 0.57 days per decade later and 0.63 days per decade earlier during the periods of 1846-1995 (Magnuson et al., 2000; Sharma et al., 2019). Changes in ice characteristics and phenology have been considered as a sensitive proxy for global warming, which could be attributed to characteristics of water bodies, climate changes, and river discharges (Duguay et al., 2010). Northeast China belongs to one of the

45 most intense areas for climate changes (Piao et al., 2010), but limited work has been carried out on analyzing the considerable variation of ice characteristics in Northeast China, where the lakes and rivers are frozen as long as five to six months.

Along with ice phenology, ice thickness is also considered as a meaningful indicator for regional and global

50 climate changes. Various models have been implemented to derive ice phenology and ice thickness, such as physically-based models, hydrodynamic models, regression models, radiation transfer model, and so on (Duguay et al., 2015). These models considered the energy exchange and physical changes of freshwater ice and required detailed ice measurements, which were carried out around the river mouth and specific rivers (Duguay et al., 2003). Most commonly used ice observations include regular observation, ice charts,

55 volunteer monitoring and field measurements (Duguay et al., 2015). The uneven distribution of hydrological stations limits the expansion of field measurement to regional and global applications. Remote sensing data have been widely used in deriving ice phenology, and ice thickness (Brown and Duguay, 2010; Dörnhöfer and Oppelt, 2016; Šmejkalová et al., 2016; Song et al., 2014), and its inability is limited by the temporal and spatial resolution of remote sensing image. Not only modeling but also remote sensing monitoring requires

60 sufficient historical ice records to validate and improve the accuracy and reliability. Most commonly used ice observations include regular observation, ice charts, volunteer monitoring and field measurements (Duguay et al., 2015). If the sample size of ice records is big enough, monitoring spatiotemporal variations of ice characteristics and the regional trend is essential and feasible, which could provide the potential for analyzing the ice phenology in specific waterbodies.

65 The most commonly vertical structure of ice cover is made up of congelation ice, snow-ice, snow, and water (Leppäranta, 2010). The ice cover of waterbodies is experiencing three stages: freeze-up, ice growth, and break-up, during which ice phenology, ice thickness, and ice composition changes greatly (Duguay et al., 2015). The effect of snow depth and air temperature on ice thickens has been analyzed based on numerous models, such as regression models (Palecki and Barry, 1986; Williams and Stefan, 2006), thermodynamic ice

70 model (Ménard et al., 2002b), and artificial neural networks (Seidou et al., 2006; Zaier et al., 2010). The most commonly vertical structure of ice cover consists of congelation ice, snow-ice, snow and water (Leppäranta, 2010). Snow depth on ice and air temperature mainly controls the total ice thickness covering congelation ice and snow-ice. Snow on ice is a good insulator and has two-fold effects: during the freeze-up process and ice growth, the timing and amount of snow directly influence the ice thickness and promote ice thickening; during

75 the break-up process, the snow has a lower light-transmitting property and prevents the ice from melting. Generally, snow depth plays a more crucial role than air temperature (Morris et al., 2005) and increasing snow depth provide favorable condition for thicker ice cover. In comparison with other works, the air temperature had more effect on ice thickness than snow depth and attributed this to the high snowfall of study

area (Gao and Stefan, 2004). Whether snow depth or air temperature is the primary factor influencing ice

80   formation and decay deserves further exploring in Northeast China.

The surface-based networks, including climatic and hydrological stations, have been established for tracing climate and hydrological changes in Northeast China, which are limited by the accessibility of surface-based networks and the range of filed measurement. The previous work explored the ice process in at one or more locations on a given river and ignored the changing regional pattern of ice development. The objectives of

85   this study are to (1) examine and compare ice phenology dynamics of three sub-basins of Songhua River from 2010 to 2015; (2) explore the relationship between ice thickness and ice phenology; (3) explore the primary factor influencing ice process and ice thickness.

2 Materials and methods

2.1 Study area

90   Songhua River Basin (119°25′-134°00′E, 41°41′-51°38′N) located in the middle of Northeast China (Figure 1) involving Jilin Province, Heilongjiang Province, and eastern part of Inner Mongolia Autonomous Region. The Songhua River (SHR) is the third-longest river in China, covering three main streams: Nenjiang, Songhua River, and Second Songhua River (Zhao et al., 2018). According to the spatial distribution of three rivers' basin, the corresponding basins include Nenjiang Basin (NJ), the Downstream Songhua River Basin (SD),

95   and the Upstream Songhua River Basin (SU), namely (Figure 1). The NJ has a length of 1370 km, and the corresponding drainage has an area of $2,55 \times 10^6$ thousand km^2; the MSR has a length of 939 km and the catchment named downstream Songhua River Basin (SD) has an area of 1.86×10^6 km^2; the SSHR have a length of 958 km and the catchment named upstream Songhua River Basin (SU) has an area of 6.19×10^6 km^2 (Yang et al., 2018). The whole SHR is featured by temperate and cold temperate climate with long and

100   cold winter and windy and dry spring. The air temperature has annual average values of 3 to 5℃, and the precipitation ranges from 400 to 800 cm from the southeast to the west (Wang et al., 2015).

[Figure 1 is added here]

2.2 Data Source

The in-situ lake ice records were available from the annual hydrological report provided by the Chinese

105   Ministry of Water Resources from 2010 to 2015, including ice phenology, ice thickness, snow depth on ice, and air temperature on bank (BAT). In-situ measurements provide five lake ice phenological events: freeze-up start (FUS), freeze-up end (FUE), break-up start (BUS), break-up end (BUE) and complete frozen duration (CFD). FUS is considered as the first day when ice can be observed; FUE is considered as the day when the surface is mainly covered by ice with open water less than 20% of view range; BUS is considered as the first

110   day when ice began to melt, and BUE is considered as the day when the surface is mainly covered by open water with ice area less than 20% of view range. CFD is the ice cover duration between FUE and BUS when the lake is completely frozen during the winter. The yearly maximum ice thickness (MIT) of the river center was involved in this paper, as well as the corresponding day of year (DOY). The average snow depth (ASD) is calculated from the mean values of 3 or 4 measurements around the ice hole for ice thickness measurement

115 without human disturbance. The measurement was carried out every five days and lasted from November to

April in cold season every year, totally 37 measurements in one cold season.

2.3 Data analysis

2.3.1 Rotated empirical orthogonal function (REOF)

Empirical orthogonal function (EOF) decomposition is commonly used in the climatic and hydrological

120 analysis (Bian et al., 2019; Yang et al., 2017), whose basic principle is to decompose the field containing p

spatial points (variable) to decompose over time. If the sample size is n, then the data value x_{ij} including

specific spatial point i and specific time j in the field can be regarded as the linear combination of spatial

function S_{ik} and time function t_{kj} ($k = 1,2,..., p$), and the equation is listed as below.

$$x_{ij} = s_{ik} \times t_{kj}$$

125 Rotated empirical orthogonal function (REOF) rotates the original EOF matrix to a new matrix that the

squared elements of eigenvectors are maximum, which could reflect the change of different geographic

regions and correlation distribution.

$$S_{b^2}^2 = \frac{1}{mM} \sum_{j=1}^{M} \sum_{p=1}^{m} (b_{jp}^2 - \overline{b^2})^2$$

b_{jp} is the j th loading coefficient of the p th EOF mode. The paper presented the first four load vectors of

130 CFD decomposed by REOF and their corresponding principal components to identify the typical

geographic zones in Northeast China.

2.3.2 Kriging

As a spatial interpolation, Kriging has been widely used to produce the spatial distribution of ice phenology

based on in-situ measurement (Choiński et al., 2015; Jenson et al., 2007). Kriging estimate the unknown

135 values based on best linear unbiased estimator with minimal variance, is expressed as:

$$\hat{Z}(s_o) = \sum_{i=1}^{N} \lambda_i Z(s_i)$$

where $\hat{Z}(s_o)$ is the estimate by Kriging at an unknown point s_o, $Z(s_i)$ is the variable at a measured point

s_i, N is the amount of measured point. λ_i is a weight for $Z(s_i)$, and relies on the arrangement of measured

values and the distance between the prediction location and measured location(C.R. Paramasivam, 2019).

140 Average values of fiver ice phenology during the six years were used to interpolate and to create the isophenes

that were contour lines connecting locations with the same ice phenology.

2.3.3 Partial least squares regression

Partial least squares regression predicts the response of Y to X data. The method decomposes the X and Y

145 data into scores and loadings and makes the correlation between different scores maximum. In this paper, Y

data is maximum ice thickness, and X data includes snow depth on ice and air temperature on bank. Besides,

Pearson correlation was conducted to analyze the relationship among five ice phenology and ice-related

parameters, including MIT, ASD, and BAT (Gao and Stefan, 1999; Williams et al., 2004).

3 Result and Discussion

150 Five ice phenology and ice thickness described the ice condition during the freeze-up process and break-up process, and the relation between ice phenology, ice thickness, and snow depth and air temperature on bank were analyzed herein.

3.1 Spatial distribution of ice process

3.1.1 The spatial distribution of ice phenology

155 Figure 2 illustrates the spatial distribution of FUS and FUE interpolated by Kriging and the isosphere in the Songhua River basin of Northeast China from 2010 to 2015. Figure 3 illustrates the spatial distribution of the BUS and BUE. The corresponding statistics are listed in Table 1. FUS ranged from October 28th to November 21st with the mean value of November 7th, and FUE ranged from November 7th to December 8th with the mean value of November 22nd. BUS ranged from March 24th to April 20th with the mean value of April 9th, and

160 BUE ranged from March 31th to April 27th with the mean value of April 15th. These four parameters showed latitudinal distribution: FUS and FUE decreased while BUS and BUE increased as the latitude increased except in NJ. The middle part on NJ had the highest FUS and FUE and decreased to the southern and northern part, which could be observed from the DOY of isophane. BUS and BUE of the middle NJ didn't show a similar pattern in Figure 3.

165 [Figure 2 and 3 is added here]

[Table 1 is added here]

Figure 4(a) illustrates the spatial distribution of CFD interpolated by Kriging and the isosphere in the Songhua River basin from 2010 to 2015. CFD ranged from 110.74 to 163.00 days with the mean value of 137.86 days, which increased from south to north as the latitude increased. Interestingly, the isophere of CFD had a

170 changing direction increasing from the southeast to northwest, which could also be found in the other four ice phenology. Both FUS and FUE negatively correlated with latitude, with coefficients of -0.66 and -0.53, namely (n=158, p < 0.001). All of BUS, BUE and CFD have positive coefficients with latitude with values of 0.48, 0.57 and 0.55 respectively (n=158, p < 0.001). High values indicated appearance delay for ice phenology The general spatial trend could be seen that the FUS and FUE tended to advance as the latitude

175 increased, BUS and BUE tended to delay, and CFD tended to prolong. The decreasing solar radiation could explain this trend due to increasing latitude, which directly connected with the ice thaw and melting process.

[Figure 4 is added here]

To find the spatial distribution of ice durations, CFD is decomposed by REOF from 2010 to 2015, and the spatial distribution of first to fourth PC mode are shown in Figures 3 (c) to 3 (f) interpolated by Kriging. The

180 first to fourth principal component (PC) modes account for 45.89%, 13.22%, 12.62%, and 12.00%, respectively, with the accumulative variance of 83.73%. The PC mode data ranged from -0.22 to 0.15, and the area with high values presented a planar distribution, which were further regarded as five typical geographic zones considering the topography of Northeast China. Zone 1 was located in the Three River Plain, where Heilongjiang, Wusuli, and Songhua River converge together, identified from the first PC mode.

185 Zone 2 was located around Heaven Lake of Changbai mountain, which was located in the southernmost part with the highest elevation of 2565 meters, identified from the second PC mode. We excluded a planar distribution above Zone 2 from these zones because of the gentle terrain in the Songhua River basin. The

middle part of the Songhua River Basin accounts for a large area where no typical zones were found. The REOF was good at enhancing the high-value areas, and the PC mode data of this area around 0 were ignored.

190 Zone 3 was located on the eastern edge of the three basins with relatively high elevation along the ridge of Changbai mountain, identified from the third PC mode. Based on the fourth PC mode, Zone 4 was determined in the northernmost part along the ridge of Xiao Higgan Mountain, where meet with Da Higgan Mountain. Zone 5 almost covered the southern part of the NJ basin along the ridge of Da Higgan Mountain and appeared in the second, third, and fourth PC. The final distribution was identified from the convergence area of these

195 three modes.

3.1.2 The spatial distribution of ice thickness

Figure 5 illustrates the spatial distribution of yearly maximum ice thickness (MIT) of the river center and the corresponding day of year (DOY). Table 1 summarized the statistical result of MIT and the DOY. Only 55, 28, and 37 stations in the SD, SU, and NJ basins were used in Figure 5 because both MIT and DOY were

200 available only 120 of 158 stations. MIT ranged from 12 cm to 146 cm, with an average value of 78 cm. The MIT between 76 and 100 cm accounted for the largest percentage of 43.33%, followed by 31.67% of MIT between 50 and 75 cm. Five stations had the MIT over than 125cm. Two stations were located in Zone 3, and three stations in Zone 4, respectively. DOY of MIT had an average value of February 21st, and MIT mainly occurred 59 and 40 times in February and March, respectively. Four of the five highest MITs over 125 cm

205 happened in March, which is consistent with inter-annual changes in ice development in Figure 6. The results suggested the river ice is always thickest and most steady in February or March, which is the best suitable time for human activities such as ice fishing and entertainment.

[Figure 5 is added here]

Figure 6 displays the interannual changes of ice development using maximum ice thickness, average snow

210 depth on ice, and air temperature on bank. Among three basins, NJ had the highest snow depth of -29.15 ± 9.99℃, followed by -25.61 ± 9.02 ℃ in the SD, then -22.17 ± 7.33 cm in the SU. SD had the highest snow depth of 9.18 cm ± 3.39 cm on average level, followed by 8.35 cm ± 4.60 cm in SU, then 8.23cm ± 3.92 cm in NJ. The changes in MIT and ASD had similar overall trend, while air temperature on bank followed the opposite trend. Both MIT and ASD went up since November and reached the peak in Marth, then dropped at

215 the begging of April. The ASD showed an obvious trend and reached the bottom in the middle of January, which is earlier than the peaks of MIT and ASD. The NJ and the SD underwent greater fluctuations than the SU, because river ice may freeze and thaw alternatively under relatively low temperature. The changes of ice characteristics differed greatly due to time and location (Hawley et al., 2018); analysis on annual changes had not been conducted because the time series were not long enough.

220 [Figure 6 is added here]

3.2 The relationship between ice development and the impact factors

3.2.1 The influence of ice thickness on ice phenology

Figure 7 display the correlation matrix between lake ice phenology and three parameters covering ASD, BAT,

225 and MIT with a dataset size of 120. Colour intensity and the size of the ellipse are proportional to the correlation coefficients. MIT had a higher correlation with four of the five indices than that of ASD and BAT

except FUS, among which MIT and BUE had the highest correlation of 0.63 (p<0.01, n=120). During the freeze-up process, two freeze-up dates had a negative correlation with MIT and ASD; during the break-up dates, two break-up dates had a positive correlation with MIT and ASD. CFD had a positive correlation with

230   MIT and ASD. The situation of BAT is contrary to that of MIT and ASD. Figure 8 shows the bivariate scatter plots between yearly maximum ice thickness (MIT) and five ice phenology. From Figure 7, the break-up process had a negative correlation with MIT, while the freeze-up had a positive correlation. Besides, the break-up process had a higher correlation with MIT, and BUS had the highest correlation coefficients with MIT of 0.65 (p<0.01). CFD also had a positive correlation with MIT with r =0.55 (P<0.01). It means that

235   thicker ice cover in winter lead to melting time tend to delay in spring. Thick ice cover stored high heat in winter, which takes a longer time to melt in spring.

[Figure 7 is added here]

240   [Figure 8 is added here]

3.2.2 The influence of snow and air temperature on ice thickness

Snow cover and air temperature are considered the two most domain climate factors influencing the ice process of freshwaters (Ménard et al., 2002b). Regarding to the annual changes, no significant correlation

245   had been found between snow depth and five ice phenology in Figure 7. The interannual changes of correlation coefficients between MIT and ASD, BAT were shown in Table 3 with a dataset size of 37. We calculated the means of MIT, ASD, and BAT from 120 stations on a specific day, 37 days during one cold season. The correlation coefficients between MIT and ASD increased from November to March and reached a peak of 0.75 in March when the ice is thickest around the year. This indicated an increasing import role of

250   snow depth on ice thickness as the ice accumulated. The higher correlation coefficients between MIT and BAT in November and December revealed that the BAT played a more important role in the freeze-up process. Besides, we found the relationship between these three parameters relied on whether the status of river ice is steady or not. We excluded the data of April in Table 2 because the river melts and refreeze alternatively during April, and the status of river ice was not steady and accurate enough.

255   Moreover, the regression equation between MIT, ASD, and BAT had been built up to quantificationally analyze their relationship. Figure 9(a) shows the scatter plot between MIT and ASD, and a linear regression function was found between MIT and ASD with a mean root square of 0.94. This showed that snow played a crucial role in the river ice decay and formation, which is consistent with previous works (Duguay et al., 2003; Ménard et al., 2002a). The positive correlation coefficient between snow depth and ice thickness both

260   in Table 2 and revealed two opposite effects of snow depth during ice development: during the ice-growth process, the snow depth protects the ice from cold air and slow down the growth rate of ice thickness (Adams and Roulet, 1980); during ice-decay process, the bottom of lake ice stopped to grow, and the snow mixed with surface ice into slushing and promoted the melting process.

265   [Figure 9 is added here]

Figure 9(b) shows the scatter plot between MIT and BAT, and an exponential function was built between MIT and BAT with a mean root square of 0.31. A monotonic function with a decreasing trend could not explain the relationship between MIT and BAT due to low R^2. Regarding interannual changes in Figure7, there existed a time lag between the peaks of MIT and BAT. The correlation coefficients of BAT exhibited a decreasing trend from November to March, which indicated a stronger role of BAT in the freeze-up process. Higher correlation coefficients of average SD, the existence of ice was more dependent on snow depth especially when the ice is thick and steady enough. The surface snow and ice melted and refroze alternatively throughout the whole ice development, particularly for the snow seen in Figure 6. Comparing the results in Table 3 and Figure 6, the air temperature had a higher correlation with ice phenology than ice thickness. The SD has a higher correlation with FUE, BUS, and CFD in Figure 6, which described the completely frozen status of a lake with thickest ice cover. Therefore, lake ice phenology closely correlated with air temperature while ice thickness correlated with snow depth.

4 Conclusion

Five river ice phenology, including FUE, FUS, BUE, BUS, and CFD, had been investigated in the Songhua River Basin of Northeast China using in-situ measurement by the method of Kriging and REOF. The FUS and FUE decreased as while the BUS, BUE, and CFD increased as the latitude increased. Five river ice phenology showed the latitudinal distribution and a changing direction from southeast to northwest. The highest MIT over 125cm were distributed along the ridge of Da Hagan Lin and Changbai Mount, and MIT occurred most often in February and March, which indicated human activities such as navigation and winter recreation are safest. Five typical geographic zones were identified from the first four PC modes of CFD, covering Changbai Mount, Three River Plain, Da Higgan Mountain, and Xiao Higgan Mountain, which provide a deeper understanding of rive ice distribution and the relationship with geographic locations and topography in Northeast China.

The interannual changes of MIT, ASD, and BAT are analyzed based on their time series. Within one cold season, MIT and ASD showed similar interannual changes that firstly increased and then decreased, while BAT showed an opposite trend, the peaks of ASD and MIT fall behind BAT for almost one month. High correlation coefficients between MIT and five ice phenology revealed ice phenology closed related to ice thickness. MIT and ASD had as high correlation coefficients as 0.95 ($p < 0.05$) when the air temperature under freezing point, which means snow cover influence the ice thickness significantly. The correlation analysis was carried out under two cases, including geographic distribution and interannual changes, and BAT has been found more associated with ice phenology than ice thickness and snow depth. We conclude that snow depth is the primary factor influencing the ice process when compared with air temperature.

The work presented aims at exploring the regional pattern of rive ice development based on the in-situ measurement and are limited by the data accessibility. Remote sensing data could provide long-term and wide-range information for ice thickness and ice phenology since 1980, which will expand our study scopes. The work herein will provide a valuable reference for the retrieval of ice development by remote sensing. The relationship between ice thickness and air temperature can't be simulated by a linear regression model,

degree-day model, or radiation transmission model considering the thermal process of ice thawing and
305   melting will be used in future work.

Abbreviations

The following abbreviations are used in this manuscript:

ASD   Average Snow depth

BAT   Air temperature on bank

310   BUS   Break-up start

BUE   Break-up end

CFD   Completely frozen duration

EOF Empirical orthogonal function

FUS   Freeze-up start

315   FUE   Freeze-up end

NJ   Nenjiang River Basin

MIT   Maximum ice thickness

PC   Principal component

REOF Rotated empirical orthogonal function

320   SD   Downstream Songhua River Basin

SU   Upstream Songhua River Basin

Author Contribution

Song K.S. and Yang Q. designed and conducted the idea of this study. Yang Q. Wen Z.D. wrote the paper
and analyzed the data cooperatively; Hao X.H. provided value suggestion for the structure of study and paper;
325   Li W.B. and Tan Y. exerted efforts on data processing and graphing. This article is a result of collaboration
with all listed co-authors.

Competing interest

The authors reported no potential conflict of interest.

Acknowledgments

References

Adams, W. and Roulet, N.: Illustration of the roles of snow in the evolution of the winter cover of a lake,
335   Arctic, 33, 1980.

Bian, Y., Yue, J., Gao, W., Li, Z., Lu, D., Xiang, Y., and Chen, J.: Analysis of the Spatiotemporal Changes of Ice Sheet Mass and Driving Factors in Greenland, Remote Sensing, 11, 2019.

Brown, L. C. and Duguay, C. R.: The response and role of ice cover in lake-climate interactions, Progress in Physical Geography, 34, 671-704, 2010.

340   C.R. Paramasivam, S. V.: An Introduction to Various Spatial Analysis Techniques. In: GIS and Geostatistical Techniques for Groundwater Science, Senapathi Venkatramanan, M. V. P., Sang Yong Chung (Ed.), Elsevier, 2019.

Choiński, A., Ptak, M., Skowron, R., and Strzelczak, A.: Changes in ice phenology on polish lakes from 1961 to 2010 related to location and morphometry, Limnologica, 53, 42-49, 2015.

345   Dörnhöfer, K. and Oppelt, N.: Remote sensing for lake research and monitoring – Recent advances, Ecological Indicators, 64, 105-122, 2016.

Duguay, C. R., Bernier, M., Gauthier, Y., and Kouraev, A.: Remote sensing of lake and river ice, 2015.

Duguay, C. R., Flato, G. M., Jeffries, M. O., Ménard, P., Morris, K., and Rouse, W. R.: Ice-cover variability on shallow lakes at high latitudes: model simulations and observations, Hydrological Processes, 17, 3465-

350   3483, 2003.

Duguay, C. R., Prowse, T. D., Bonsal, B. R., Brown, R. D., Lacroix, M. P., and Ménard, P.: Recent Trends in Canadian Lake Ice Cover, Hydrological Processes, 20, 781-801, 2010.

Gao, B. S. and Stefan, H. G.: Multiple linear regression for lake ice and lake temperature characterisitcs, Journal of Cold Regions Engineering, 13, 59-77, 1999.

355   Gao, S. and Stefan, H. G.: Potential Climate Change Effects on Ice Covers of Five Freshwater Lakes, Journal of Hydrologic Engineering, 9, 226-234, 2004.

Hampton, S. E., Galloway, A. W., Powers, S. M., Ozersky, T., Woo, K. H., Batt, R. D., Labou, S. G., O'Reilly, C. M., Sharma, S., Lottig, N. R., Stanley, E. H., North, R. L., Stockwell, J. D., Adrian, R., Weyhenmeyer, G. A., Arvola, L., Baulch, H. M., Bertani, I., Bowman, L. L., Jr., Carey, C. C., Catalan, J., Colom-Montero, W.,

360   Domine, L. M., Felip, M., Granados, I., Gries, C., Grossart, H. P., Haberman, J., Haldna, M., Hayden, B., Higgins, S. N., Jolley, J. C., Kahilainen, K. K., Kaup, E., Kehoe, M. J., MacIntyre, S., Mackay, A. W., Mariash, H. L., McKay, R. M., Nixdorf, B., Noges, P., Noges, T., Palmer, M., Pierson, D. C., Post, D. M., Pruett, M. J., Rautio, M., Read, J. S., Roberts, S. L., Rucker, J., Sadro, S., Silow, E. A., Smith, D. E., Sterner, R. W., Swann, G. E., Timofeyev, M. A., Toro, M., Twiss, M. R., Vogt, R. J., Watson, S. B., Whiteford, E. J.,

365   and Xenopoulos, M. A.: Ecology under lake ice, Ecol Lett, 20, 98-111, 2017.

Hawley, N., Beletsky, D., and Wang, J.: Ice thickness measurements in Lake Erie during the winter of 2010–2011, Journal of Great Lakes Research, 44, 388-397, 2018.

Jenson, B. J., Magnuson, J. J., Card, V. M., Soranno, P. A., and Stewart, K. M.: Spatial Analysis of Ice Phenology Trends across the Laurentian Great Lakes Region during a Recent Warming Period, Limnology

370   Oceanography, 52, 2013-2026, 2007.

Kwok, R. and Fahnestock, M. A.: Ice Sheet Motion and Topography from Radar Interferometry, IEEE Transactions on Geoscience Remote Sensing, 34, 189-200, 1996.

Leppäranta, M.: Modelling the Formation and Decay of Lake Ice, 2010.

Lindenschmidt, K.-E., Das, A., and Chu, T.: Air pockets and water lenses in the ice cover of the Slave River,

375   Cold Regions Science and Technology, 136, 72-80, 2017.

Magnuson, J. J., Robertson, D. M., Benson, B. J., Wynne, R. H., Livingstone, D. M., Arai, T., Assel, R. A., Barry, R. G., Card, V., and Kuusisto, E.: Historical Trends in Lake and River Ice Cover in the Northern Hemisphere, Science, 289, 1743-1746, 2000.

Ménard, P., Duguay, C. R., Flato, G. M., and Rouse, W. R.: Simulation of ice phenology on Great Slave Lake,
380 Northwest Territories, Canada, Hydrological Processes, 16, 3691-3706, 2002a.

Ménard, P., Duguay, C. R., Pivot, F. C., Flato, G. M., and Rouse, W. R.: Sensitivity of Great Slave Lake ice cover to climate variability and climatic change, New Zealand, 2nd–6th December 2002b.

Morris, K., Jeffries, M., and Duguay, C.: Model simulation of the effects of climate variability and change on lake ice in central Alaska, USA, Annals of Glaciology, 40, 113-118, 2005.

385 Palecki, M. A. and Barry, R. G.: Freeze-up and Break-up of Lakes as an Index of Temperature Changes during the Transition Seasons: A Case Study for Finland, Journal of Applied Meteorology, 25:7, 893-902, 1986.

Piao, S., Ciais, P., Huang, Y., Shen, Z., Peng, S., Li, J., Zhou, L., Liu, H., Ma, Y., Ding, Y., Friedlingstein, P., Liu, C., Tan, K., Yu, Y., Zhang, T., and Fang, J.: The impacts of climate change on water resources and
390 agriculture in China, Nature, 467, 43-51, 2010.

Seidou, O., Ouarda, T. B. M. J., Bilodeau, L., Bruneau, B., and St-Hilaire, A.: Modeling ice growth on Canadian lakes using artificial neural networks, Water Resources Research, 42, 2526-2528, 2006.

Sharma, S., Blagrave, K., Magnuson, J. J., O'Reilly, C. M., Oliver, S., Batt, R. D., Magee, M. R., Straile, D., Weyhenmeyer, G. A., Winslow, L., and Woolway, R. I.: Widespread loss of lake ice around the Northern
395 Hemisphere in a warming world, Nature Climate Change, 9, 227-231, 2019.

Shuter, B. J., Finstad, A. G., Helland, I. P., Zweimüller, I., and Hölker, F.: The role of winter phenology in shaping the ecology of freshwater fish and their sensitivities to climate change, Aquatic Sciences, 74, 637-657, 2012.

Šmejkalová, T., Edwards, M. E., and Dash, J.: Arctic lakes show strong decadal trend in earlier spring ice-
400 out, Scientific Reports, 6, 38449, 2016.

Song, C., Bo, H., Ke, L., Richards, K. S. J. I. J. o. P., and Sensing, R.: Remote sensing of alpine lake water environment changes on the Tibetan Plateau and surroundings: A review, Isprs Journal of Photogrammetry Remote Sensing, 92, 26-37, 2014.

Stephanie, J. and Stefan Heinz, G.: Indicators of climate warming in minnesota : Lake ice covers and
405 snowmelt runoff, Climatic Change, 75, 421-453, 2006.

Wang, S., Wang, Y., Ran, L., and Su, T.: Climatic and anthropogenic impacts on runoff changes in the Songhua River basin over the last 56years (1955–2010), Northeastern China, Catena, 127, 258-269, 2015.

Williams, G., Layman, K. L., and Stefan, H. G.: Dependence of lake ice covers on climatic, geographic and bathymetric variables, Cold Regions Science Technology, 40, 145-164, 2004.

410 Williams, S. G. and Stefan, H. G.: Modeling of Lake Ice Characteristics in North America using Climate, Geography, and Lake Bathymetry, Journal of Cold Regions Engineering, 20, 140-167, 2006.

Xing, F., Stefan, H. G., Williamson, C. E., Saros, J. E. G., Vincent, W. F., and Smol, J. P.: Simulations of climate effects on water temperature, dissolved oxygen, and ice and snow covers in lakes of the contiguous U.S. under past and future climate scenarios, J Limnology Oceanography, 54, 2359-2370, 2009.

415   Yang, P., Xia, J., Zhan, C., Qiao, Y., and Wang, Y.: Monitoring the spatio-temporal changes of terrestrial
       water storage using GRACE data in the Tarim River basin between 2002 and 2015, Science of the Total
       Environment, 595, 218-228, 2017.

       Yang, Q., Song, K., Hao, X., Chen, S., and Zhu, B.: An Assessment of Snow Cover Duration Variability
       Among Three Basins of Songhua River in Northeast China Using Binary Decision Tree, Chinese
420   Geographical Science, 28, 946-956, 2018.

       Zaier, I., Shu, C., Ouarda, T. B. M. J., Seidou, O., and Chebana, F.: Estimation of ice thickness on lakes using
       artificial neural network ensembles, Journal of Hydrology, 383, 330-340, 2010.

       Zhao, Y., Song, K., Lv, L., Wen, Z., Du, J., and Shang, Y.: Relationship changes between CDOM and DOC
       in the Songhua River affected by highly polluted tributary, Northeast China, Environmental Science Pollution
425   Research, 25, 25371-25382, 2018.

Tables

Table 1 Statistics summary of ice phenology interpolated by Kriging from 2010 to 2015. The ice phenology
430 including freeze-up start (FUS), freeze-up end (FUE), break-up start (BUS), break-up end (BUE), the
complete frozen duration (CFD). NJ, SD and SU represent the Nenjiang basin, the downstream Songhua
River basin (SD) and the upstream Songhua River basin (SU). DOY denotes day of year. Std Dev. denotes
standard deviation.

Basins	Statistics	FUS (DOY)	FUE (DOY)	BUS (DOY)	BUE (DOY)	CFD (day)
NJ	Maximum	319.14	334.98	110.54	117.61	163.00
	Mean	307.02	324.58	98.65	106.64	139.39
	Minimum	301.41	311.30	84.53	90.40	119.11
	Std Dev.	3.91	5.69	8.16	6.80	13.22
SD	Maximum	321.08	334.36	110.01	102.84	154.06
	Mean	313.74	326.70	102.55	97.15	140.86
	Minimum	305.64	316.80	93.22	92.37	125.32
	Std Dev.	2.83	3.13	3.92	2.12	5.69
SU	Maximum	325.92	342.09	98.25	114.37	133.62
	Mean	320.39	334.35	91.93	106.43	122.61
	Minimum	313.79	327.68	83.46	95.69	110.74
	Std Dev.	2.34	3.09	3.21	4.24	4.85
Total	Maximum	325.92	342.09	110.54	117.61	163.00
	Mean	311.16	326.58	99.25	105.38	137.86
	Minimum	301.41	311.30	83.46	90.40	110.74
	Std Dev.	5.74	5.54	7.17	6.34	11.68

Table 2 The Frequency of yearly maximum ice thickness from November to April. The row represents
435 different year in cold season and the column represents yearly maximum ice thickness with the unit of cm.

MIT \ Month	<50	50-75	76-100	101-125	125-150
December	4	1	0	1	0
January	4	4	1	0	0
February	4	25	26	3	1
March	1	3	24	8	4
April	0	2	1	0	0
After April	0	3	0	0	0
Total	13	38	52	12	5

Table 3 Correlation coefficient between maximum ice thickness (MIT), average snow depth (ASD) and
air temperature on bank (BAT) with dataset size of 120. The asterisk indicates the significant level of
correlation coefficients, ** means significant at 99% level ($p<0.01$), and * means significant at 95%
level ($p<0.05$).

CC	November	December	January	February	March
MIT vs. ASD	0.17	0.66*	0.53*	0.59*	0.75**
MIT vs. BAT	-0.90**	-0.80**	-0.55*	-0.30	-0.45

440 **Figures**

DHM: Da Higgan moutain
TRP: Three River Plain
LRB: Liaohe River Basin

XHM: Xiao Higgan moutain
CBM: Changbai Mount
SHB: Songhua River Basin

HLJ: Heilongjiang River
WSL: Wusli River
YLJ: Yalvjiang River
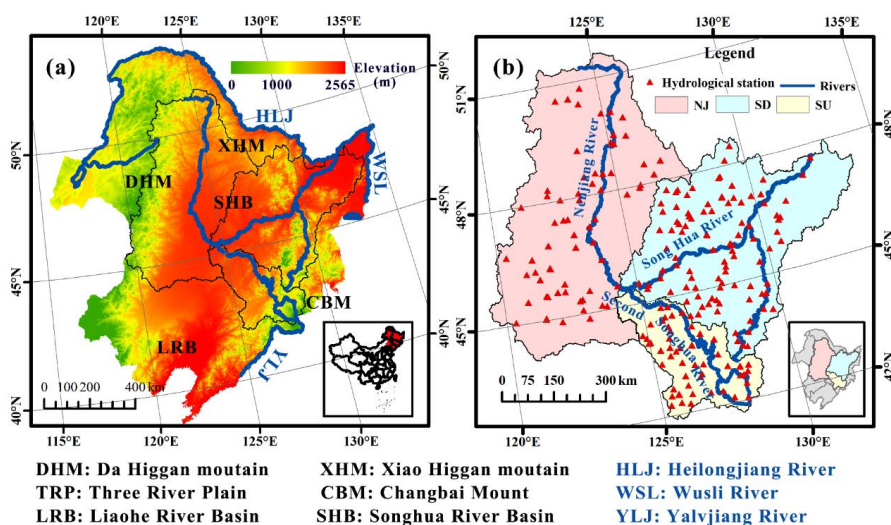
Figure 1 The geographic location of Songhua River Basin showing 158 hydrological stations. The basin includes three basins: Nenjiang River Basin (NJ), downstream Songhua River Basin (SD) and upstream Songhua River Basin (SU). The elevation is provided by Shuttle Radar Topography Mission (SRTM)
445   with spatial resolution of 90 meters.
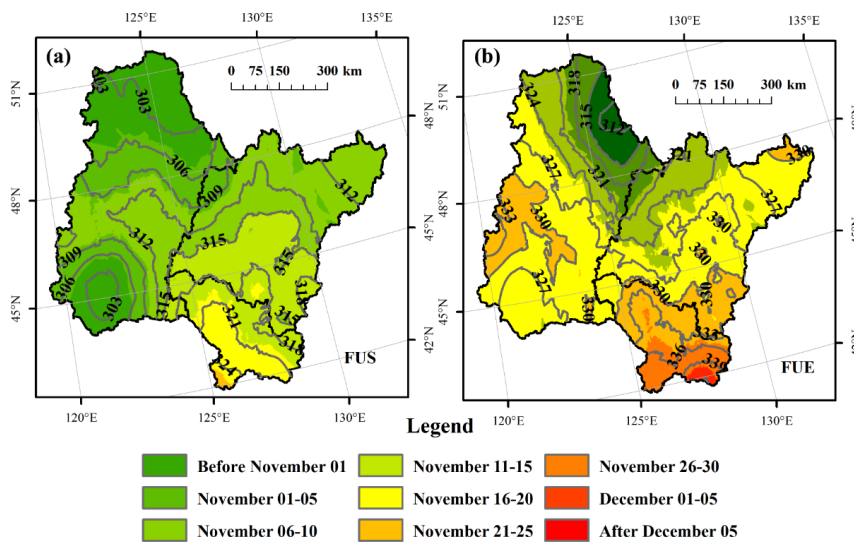
Figure 2 The spatial distribution of freeze-up start (FUS) and freeze-up end (FUE) in the Songhua River
basin of Northeast China from 2010 to 2015. The number labelled indicates the day of year (DOY) of
isophene.
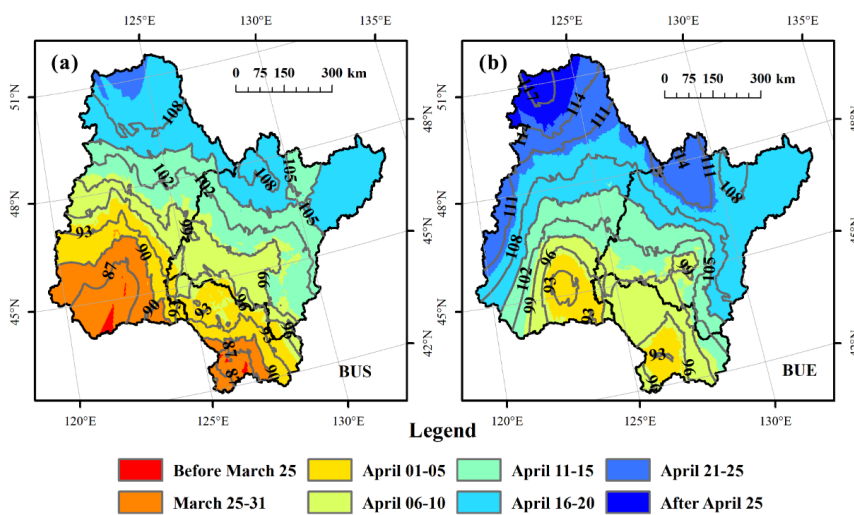
Figure 3 The spatial distribution of break-up start (BUS) and break-up end (BUE) in the Songhua River
basin of Northeast China from 2010 to 2015. The number labelled indicates the day of year (DOY) of
isophene.
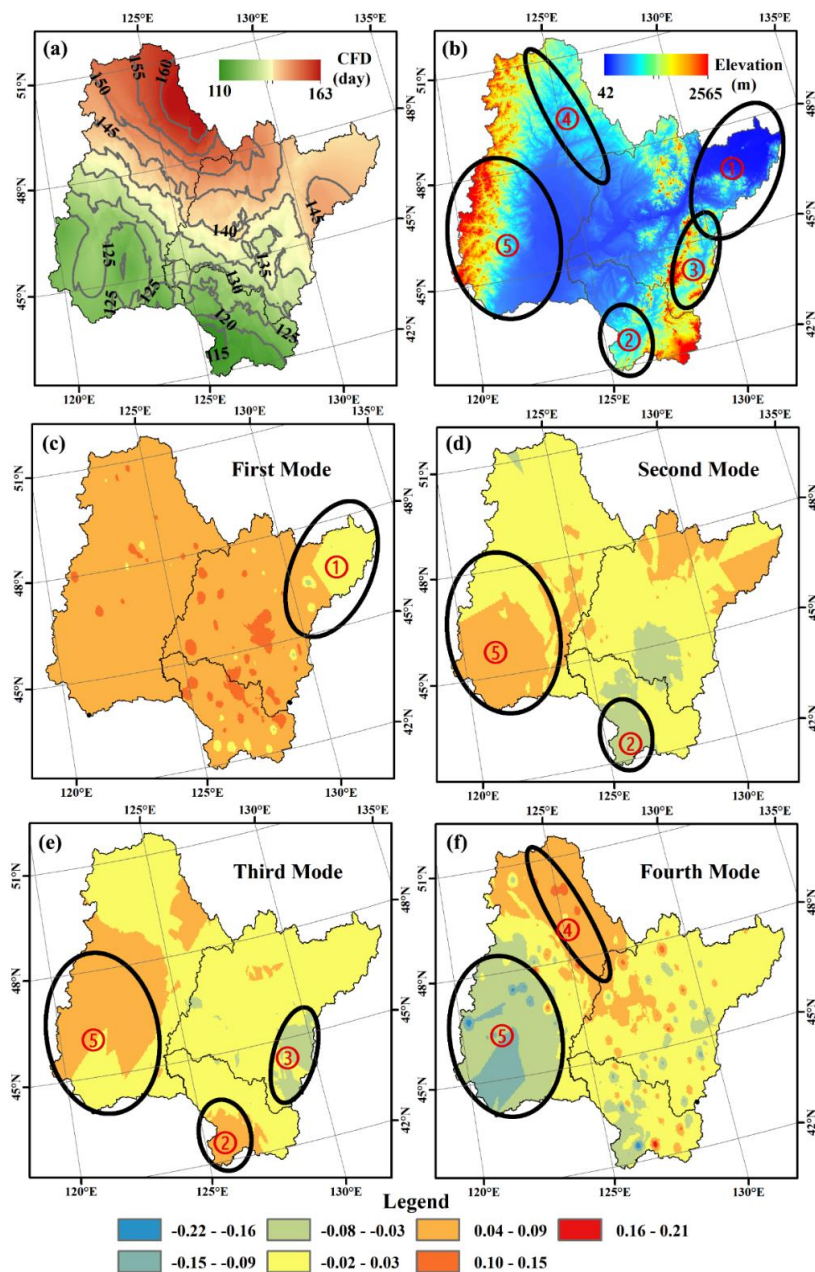
Figure 4 The spatial distribution of complete frozen duration (CFD) (a), five typical geographical zones
(b), and fist four principal components (c-f) of decomposed by rotated empirical orthogonal function
460 (REOF) in the Songhua River basin of Northeast China.
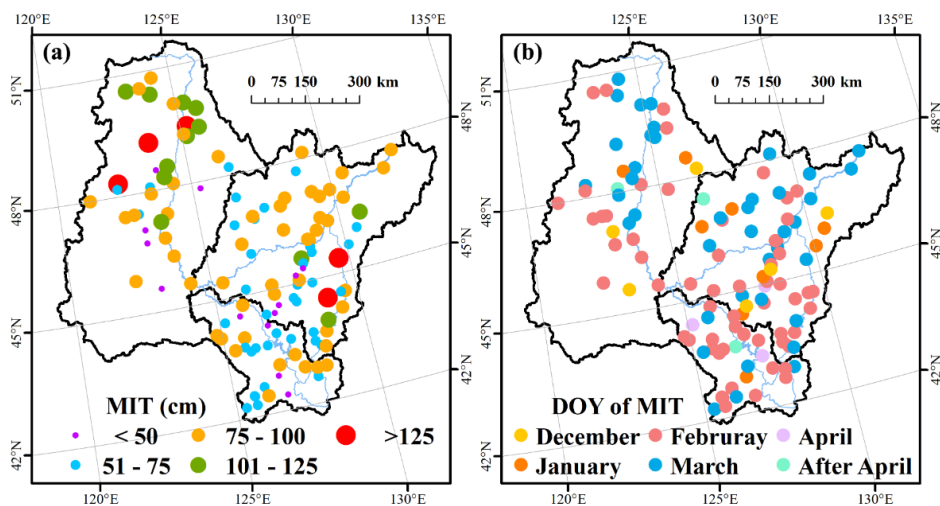
Figure 5 The spatial distribution of yearly maximum ice thickness (MIT) of river centre and the corresponding year of day (DOY).
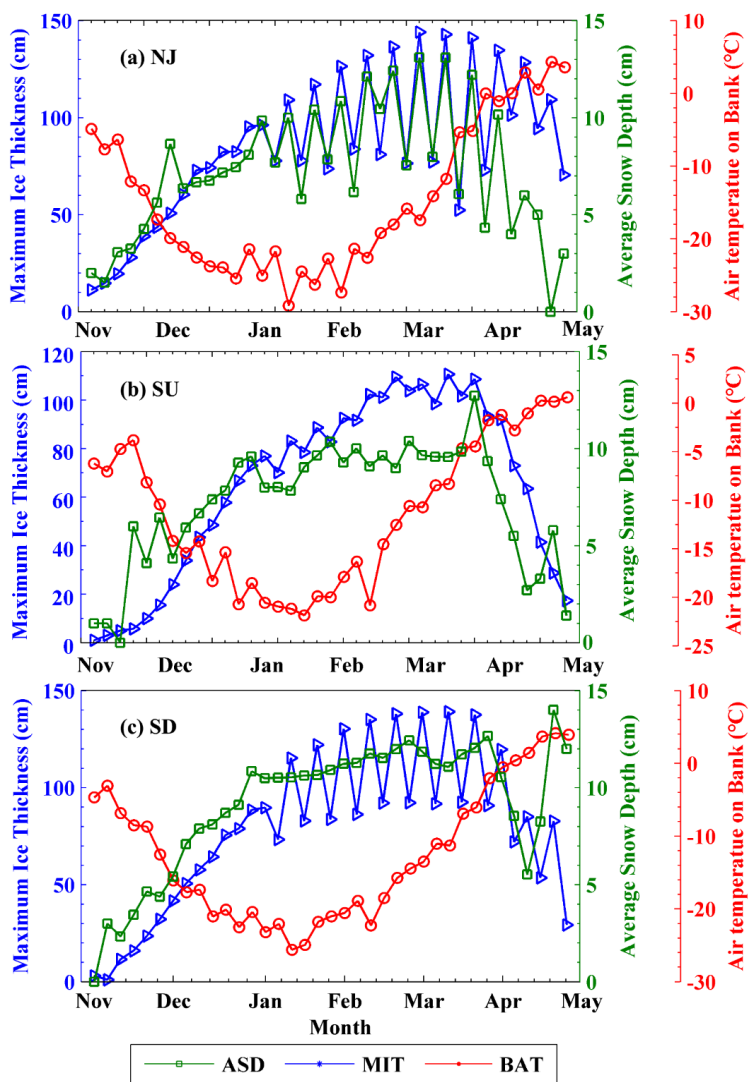
465

Figure 6 The time series of yearly maximum ice thickness (MIT), average snow depth (ASD) and air temperature on bank (BAT) from November to April during 2010-2015.

470
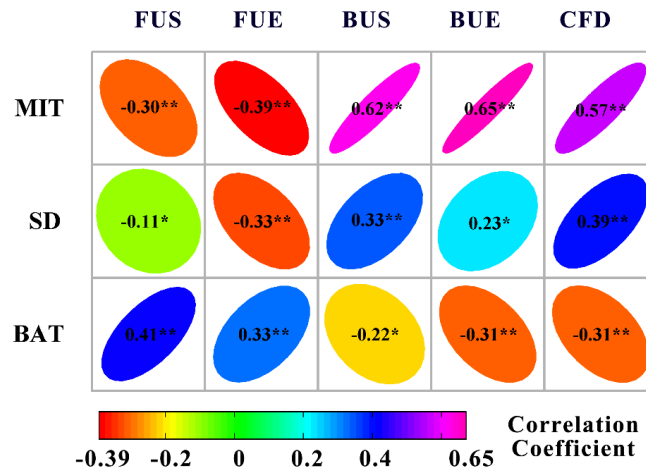
Figure 7 Correlation matrix between maximum ice thickness (MIT), average snow depth (ASD) and air temperature on bank (BAT) and lake ice phenology with dataset size of 120. The asterisk indicates the
475 significant level of correlation coefficients, ** means significant at 99% level (p<0.01), and * means significant at 95% level (p<0.05).

FUS = -0.01 × MIT + 321.29
r = -0.30, p < 0.01
FUE = -0.14 × MIT + 338.56
r = -0.39, p < 0.01
BUS = 0.24 × MIT + 79.94
r = 0.62, p < 0.01
BUE = 0.22 × MIT + 86.08
r = 0.65, p < 0.01
CFD = 0.39 × MIT + 106.06
r = 0.57, p < 0.01
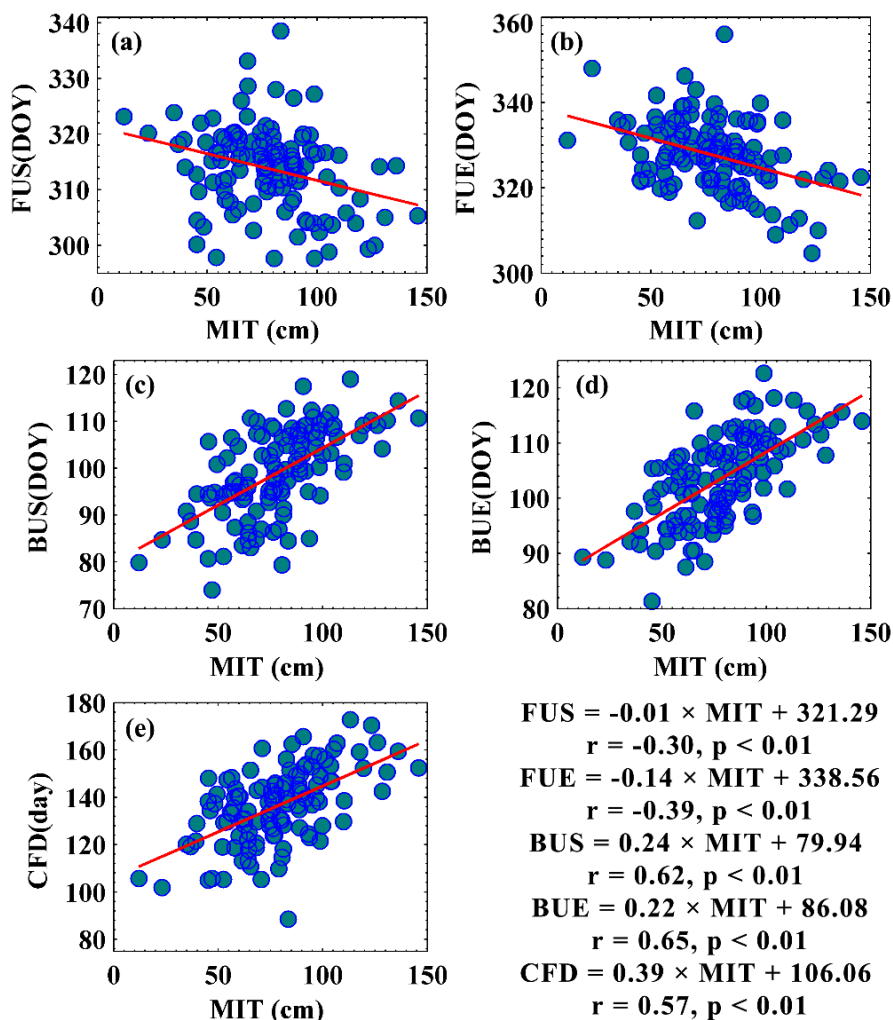
480 Figure 8 The bivariate scatter plots with linear regression lines between yearly maximum ice thickness (MIT) and ice phenology with dataset size of 120, *r* and *p* denote the corresponding correlation coefficient and *p* value of regression line. The ice phenology includes freeze-up start (FUS), freeze-up end (FUE), break-up start (BUS), break-up end (BUE) and complete frozen duration (CFD).

485
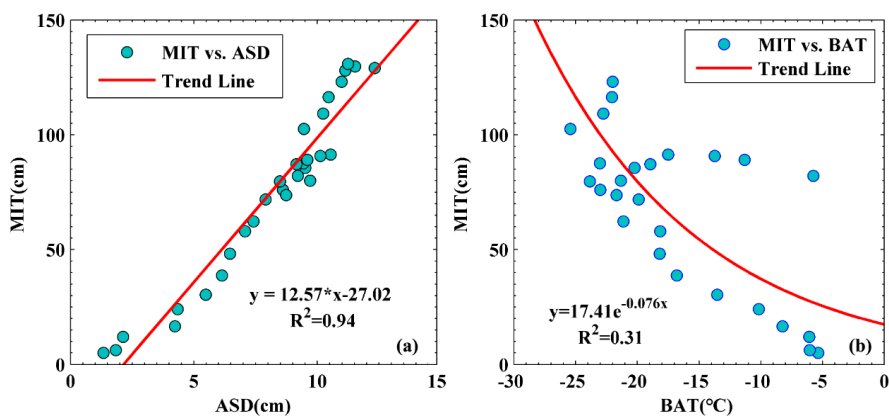
Figure 9 The scatter plot between maximum ice thickness (MIT), average snow depth (ASD) and air temperature on bank (BAT) and the corresponding trend line. The data was selected under the criteria with air temperature below 2℃ and snow depth less than 20 cm.